lajss.org© Latin American Journal of Solids and Structures

www.lajss.org

Experimental results on the damping ratio in sample of a real umbilical

Luiz G. de O. Appel[a]*, Lívia R. Bozzo[a], Gabriel de P. Dittrich[a], André L. C. Fujarra[a], Thiago A. Fiorentin[a], Andrea P. Carboni[a], Marcos A. Rabelo[a], Fabio P. S. Mineiro[b], Carlos A. D. Lemos[b]

[a] Department of Mobility Engineering, Federal University of Santa Catarina, Estr. Dona Francisca 8300, Joinville, 89219-600, Santa Catarina, Brazil. Email: appelluiz@gmail.com, liviabozzo@gmail.com, gabrieldittrich15@gmail.com, andre.fujarra@ufsc.br, thiago.antonio@ufsc.br, andrea.piga@ufsc.br, marcos.rabelo@ufsc.br

[b] Tecnologia de Risers e Submarinos, PETROBRAS, Av. Horácio Macedo 950, Rio de Janeiro, 21941-915, Rio de Janeiro, Brazil. Email: fabiomineiro@petrobras.com, caolemos@petrobras.com

*Corresponding author

https://doi.org/10.1590/1679-7825/e8807

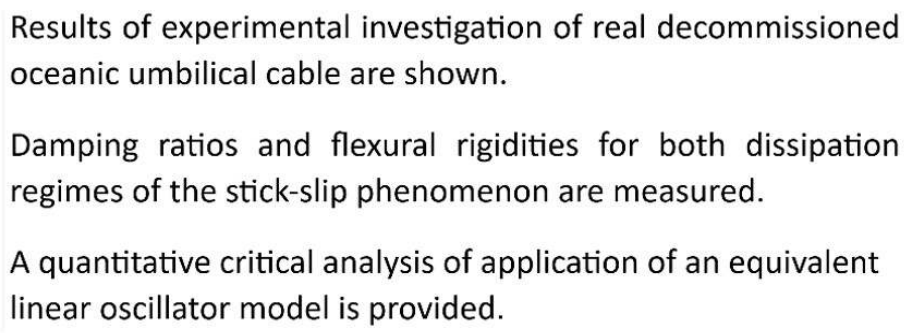
Abstract

The operation of offshore platforms depends on the functions performed by umbilical cables, among other structures. These slender multi-layered structures are designed to resist stresses imposed on them by the sea current and movement of the free-surface platform. Therefore, design interest lies on knowledge regarding their dynamic behaviour, in particular, their damping properties. The present work aims to experimentally characterize the structural damping ratio of a 6-meter long sample of a real umbilical cable, by means of decay tests and cyclical bending tests in air. Two dissipation regimes were observed during the decay tests. The most intense one, characterized by internal accommodation, is preponderant for larger displacements. It induces substantial increases in the damping ratio and natural oscillation period. The cyclical bending test corroborate this scenario. Furthermore, an assessment of the model applied to evaluate the damping ratio from the bilinear hysteretic cycle revealed an overestimation of this quantity for large pos-slip displacements. A correction is proposed.

Keywords

Offshore Structures, Unbonded Flexible Pipe Dynamics, Damping, Decay Tests, Cyclical Bending Tests.

Graphical Abstract



Received August 14, 2025. In revised form October 01, 2025. Accepted October 22, 2025. Available online October 29, 2025.
https://doi.org/10.1590/1679-7825/e8807

Latin American Journal of Solids and Structures. ISSN 1679-7825. Copyright © 2026. This is an Open Access article distributed under the terms of the Creative Commons Attribution License, which permits unrestricted use, distribution, and reproduction in any medium, provided the original work is properly cited.

1 INTRODUCTION

In the field of Ocean Engineering, umbilical cables allow for the communication between the platform on the air water interface and the equipment installed on the seabed hundreds if not thousands of meters below. These cables support the pathways for the transfer of electrical signals and work fluid between these stations. Architecturally, they are classified as slender unbonded pipes, for their internal components (structural or otherwise) are not solidary, i.e., relative displacement between them may occur.

Due to their extreme lengths, total weight and adverse environmental conditions they withstand, installation and maintenance operations are very logistically demanding. Therefore, design for fatigue resistance is paramount, especially considering the catastrophic environmental, human, economic and political toll in the event of a structural failure.

In this context, it is known that the amplitudes and, consequently, the stresses imposed to these structures are dominated by damping properties (Pesce, 1997), of which there are three sources: (i) hydrodynamic, from interaction with the current around the pipe, (ii) viscoelastic, and (iii) frictional and strain-bound, from internal accommodation between the components.

The larger fraction of the research, as it stands at the time of writing, investigates the first source, probably since current-structure interaction has larger implications on global pipe and surface superstructure dynamics and operate over larger loads (Pesce, Martins and Chakrabarti, 2005).

A less voluminous body of work dedicates itself to quantify the two latter effects and discuss the specific structural mechanisms that produce them (Witz and Tan, 1992; Fang and Lyons 1992; Kraincanic and Kebadze, 2001), as well as descriptions and discussion of the models suitable to their analysis (Hudson, 1965; Bech and Skallerud, 1992). On this front, the focus of means of investigation has been recently shifting slightly in favor of analytical-numerical, FEM-based and FEM-calibrated analytical incursions (Alfano, Bahtui and Bahai, 2009) which allow for more variance in parameter setting, such as internal pressure and axial load (Li, Xu and Zhang, 2013a), material composition, structural configuration (Ma et al, 2022), stress-state determination for more complex load compositions (Li, Xu and Zhang, 2013b; Dong et al, 2013) and parametric time- (Santos et al, 2015; Liu et al, 2020) or temperature dependency (Liu and Vaz, 2016), as well as modelling of displacement and strain of individual structural components (Wang and Yue, 2021).

The present work then aims to provide renewed experimental data to this panorama. Here, the combination of the two latter mentioned dissipation sources is assessed by means of free-decay and cyclical bending tests of a sample of a decommissioned umbilical cable.

The article comprises four sections. The present one sets the context of the field of research and relevance of this work. The next presents the umbilical cable sample and its main characteristics, the testing matrix, environment and equipment, as well as the methods of analysis. From there follows the presentation of results, in all detail for some representative cases and general overview for the remaining repetitions. Descriptions and discussion are provided alongside, tracing comparisons and remarks on method applicability and efficacy. The document then concludes with a brief overall review and synthesis of results and contribution.

2 METHODOLOGY

The test matrix is comprised, for the decay tests, of 4 initial conditions, for each one 3 repetitions, totaling here 12 tests. Tests were conducted on a 6 m long, 129 mm nominal external diameter span of decommissioned umbilical cable, of mass per unit length 27.9 kg/m, hung vertically, both ends secured by stainless steel connectors. These ensured inter-component bonding at the extremities. The connectors measured 379 mm in length and 255 mm in diameter, each of mass 110 kg. The cable was comprised of an outer polymeric sheath, a pair of counterwound layers of steel helical tendons and over a dozen smaller interlocked fluid conduits and electrical cables of varying diameters. The set (cable and connectors) was mounted in a clamped-free configuration. Displacement time-series were acquired by means of a Micro-Epsilon WDS 500 P60 Industrial Draw-Wire sensor. An acquisition frequency of 100 Hz was used for all tests, of which the maximum relevant frequency did not surpass 3 Hz. Therefore, no aliasing is present in the output data.

For the cyclical bending tests, a similar configuration was adopted, this time reducing the vertical free-span to 1.2, m. A hydraulic actuator was then mounted transversely to the structure, imposing a period and amplitude-controlled sinusoidal displacement to the free end of the cable. Force-displacement time series were delivered by the actuator system. Multiple hysteretic cycles were measured for 3 amplitudes: 70, 140 and 200 mm; with respective periods of 10, 80 and 114 s.

Graphical descriptions of the testing structures and equipment are provided in Figures 1, 2 and 3 below.

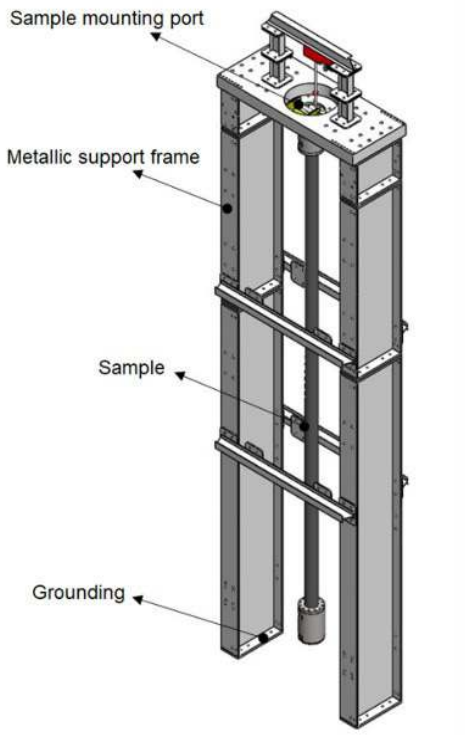


Figure 1 Assembly design: structure for decay tests. Courtesy of STRESSTEC Engenharia.

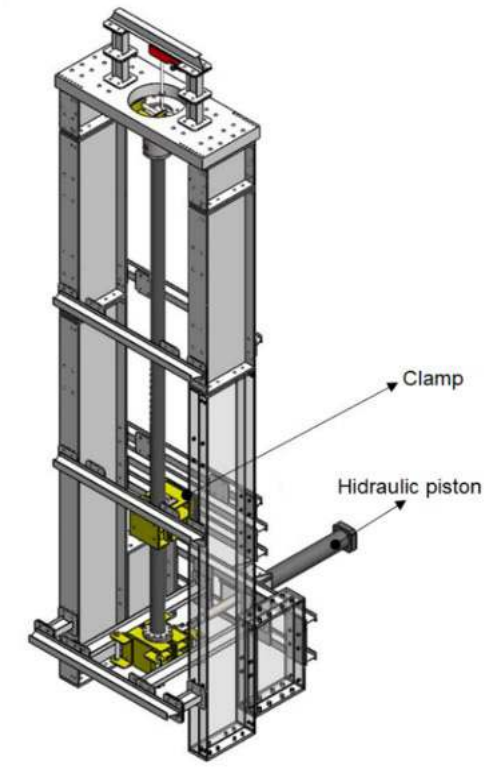


Figure 2 Assembly design: structure for cyclical bending tests. Courtesy of STRESSTEC Engenharia.



Figure 3 Detail of stainless-steel connector mounted at the free end of the umbilical cable sample. Courtesy of STRESSTEC Engenharia.

Regarding data processing and analysis of the test outputs, Damped Single Degree of Freedom Oscillator model is applied. Exponentially decaying oscillatory response is observed, hence, quantification of system parameters occurs through the lens of the transient sub-critically damped solution. Three techniques are implemented in GNU Octave: (Tech-A) Logarithmic Decrement, (Tech-B) Peaks and Troughs Linear Least Squares Approximation, (Tech-C) Envelope Linear Least Squares Approximation.

Theoretical basis for the damping ratio evaluation is sourced from Clough and Penzien (2003). For Tech-A, the observed single-cycle damping ratios are plotted against the averaged amplitude of the respective maxima or minima from which the decrement was calculated. Tech-B and Tech-C look to infer the damping ratio by approximating the exponential envelope of the response. Technique B does so by linearizing the natural logarithm of the peaks (local maxima, positive), troughs (local minima, negative) and their superimposed absolute values, and evaluating the damping ratio from the approximation's angular coefficient. Tech-C, operates similarly, but instead of the critical points of the signal (specifically, their natural logarithm), it linearizes the natural logarithm of the upper envelope given by the absolute value of the Hilbert Transform, as laid out by Bendat and Piersol (2010).

For the cyclical bending tests, the force-displacement series were analyzed via a bilinear hysteresis model, as presented by Hudson (1965) and Bech and Skallerud (1992). Additional theoretical foundation regarding structural dynamics is drawn from the works of Fang and Lyons (1992) and Inman (2014). The mean hysteretic cycle was obtained by segregating increasing from decreasing displacement, generating the upper and lower curve of the cycle. Values of each curve were then averaged in N = 50 uniformly distributed bands in the interval between the maximum and minimum force values in the signal. Each curve was then approximated by two concatenated linear regressions. This method is hereby referred to as Double Linear Least Squares Approximation (or its acronym D-LLSA). The representative regime-transition displacement for each curve is defined for $\mathbf{x_k}$, $\boldsymbol{k} \in [\mathbf{2}, \boldsymbol{N-1}]$ such that the square deviation $\mathbf{D}(\mathbf{x_k})$ (see Eq. 1) between the average cycle and the concatenated linear regressions is minimal.

$$\mathbf{D}(\mathbf{x_k}) = \frac{1}{\mathbf{x_N} - \mathbf{x_1}} \left[\int_{\mathbf{x_1}}^{\mathbf{x_k}} \left[\boldsymbol{F}(\boldsymbol{x}) - \boldsymbol{\Lambda}_{\mathbf{x_1}}^{\mathbf{x_k}}(\boldsymbol{x}) \right]^2 \boldsymbol{dx} + \int_{\mathbf{x_k}}^{\mathbf{x_N}} \left[\boldsymbol{F}(\boldsymbol{x}) - \boldsymbol{\Lambda}_{\mathbf{x_k}}^{\mathbf{x_N}}(\boldsymbol{x}) \right]^2 \boldsymbol{dx} \right] \quad (\mathbf{1})$$

In Equation 1, $\boldsymbol{\Lambda}_{\mathbf{x_1}}^{\mathbf{x_k}}$ and $\boldsymbol{\Lambda}_{\mathbf{x_k}}^{\mathbf{x_N}}$ are, respectively, the linear regressions of the curve segments before and after the candidate displacement $\mathbf{x_k}$. Integrals are evaluated numerically using the trapezium method. From the best-fitting regression pairs for the upper and lower curves of the cycle, flexural rigidities, characteristic displacements and the equivalent damping ratio are obtained.

From the characteristic displacements (x_y - transition displacement- and x_m - amplitude) and equivalent spring constants (k_1 - pre-slip - and k_2 - post-slip) obtained from the best-fitting bilinear trajectory, the per-cycle energy dissipation can be calculated from the area within the cycle. The resulting equivalent damping ratio is given from these parameters by Hudson (1965):

$$\zeta_{eq} = \frac{2}{\pi} \frac{\left(\frac{x_m}{x_y}\right)-1}{\left(\frac{x_m}{x_y}\right)^2}\left(1-\frac{k_2}{k_1}\right) \tag{2}$$

3 RESULTS AND DISCUSSION

In this section, three cases (out of 12) are presented regarding the decay tests. The first is for a 130 mm initial displacement; the second, for a -450 mm initial displacement; and the third is the reanalysis of this very signal, now excluding the first cycle. Regarding method convergence and verisimilitude, the results displayed are representative of their peers, hence, non-disclosure seeking brevity does not suppress information relevant to the discussion that follows.

The decay results are shown as bundles of five graphs. The two on the left-hand side are, top to bottom, the displacement time-series and the Fast Fourier Transform of the signal. Peaks, troughs, ascending zeros, and the envelope obtained via Hilbert Transform are plotted over the time-series signal. The peak amplitude is highlighted on the FFT, and the peak frequency is displayed above the graph. On the right-hand side are, top to bottom again, the results of damping ratio obtained from the three techniques applied, Tech-A through Tech-C.

Proceeding to result presentation and discussion per se, Figure 4 displays the results for one of the 6 repetitions conducted for the 130 mm absolute initial displacement. The treated section of the signal begins at the first zero-crossing after release. This detail persists throughout the analysis of all signals collected. Returning to this first case, the system response closely resembles a textbook analytical solution. No apparent amplitude modulation (other than the expected exponential decay) is observed, the FFT indicates a single very pronounced dominant frequency, and the linear regressions in Tech-B and Tech-C fit their inputs closely. A slight bilateral difference is observed in the damping ratios. The evaluations deviate at most by around 1%.

Discussing minutia, note that, differently form Techs-B and C, the damping ratios obtained from the Logarithmic Decrement in Tech-A are not plotted against time, but against amplitude. Furthermore, this axis segregates mean-decrement amplitudes by sign: peaks (of "positive amplitude") on the right, in red circles; and troughs (of "negative amplitude"), on the left, in blue squares, identically to the time-series signal on the top left. That being said, the order of the measurements is not graphically displayed from left to right, but from the extremities to the centre, alternating sides. For the present test, the single-cycle damping ratios tend to decrease with amplitude, but only slightly. Individual values differ from the general mean by at most 3%.

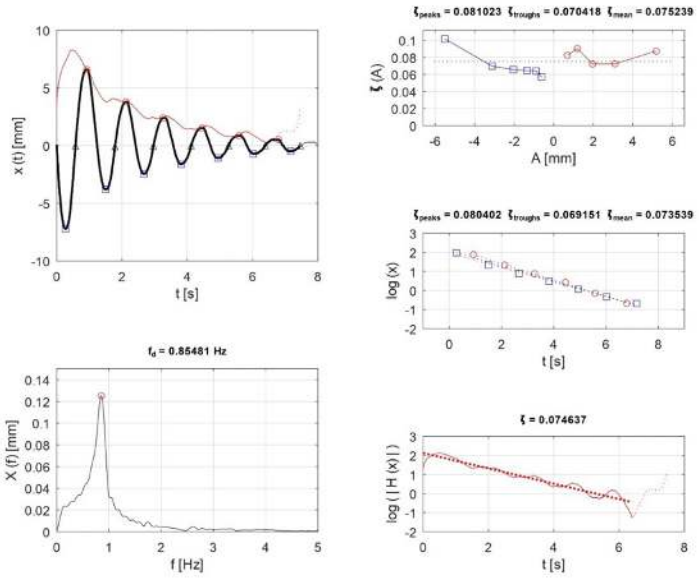


Figure 4 Umbilical cable decay test results for +130 mm initial displacement.

Taking the analysis further, Figure 5 brings forward the data obtained for one of the repetitions of the larger 450 mm amplitude decay test. The results obtained by the techniques implemented are not only different from those obtained for the 130 mm decay but more self-conflicting.

A 65% decrease in peak frequency is observed between tests. Following the applied oscillator model, this decrease may arise from three sources: (i) increased inertia; (ii), increased dissipation; or (iii) decreased restoration. No mass is added or lost during the test, hence dismissing source (i). For (ii) to be entirely responsible for this decrease, an almost unitary damping ratio would be necessary, which is far removed from the test observation and analysis. Tech-A results show maximal damping ratios for the first peak and trough of the signal of around 37%. Therefore, the reduction in frequency must be some combination of increased dissipation and decreased rigidity.

A second peak of perceptible but minute amplitude is observed around 0.8 Hz, similar to that of the first test. This is justified by an apparent decrease in the half-oscillation (peak-to-trough) period noted on the latter half of the signal. This effect is not immediately clear from the displacement time-series, despite the markings, but is more evident in the juxtaposition provided by the regression in Tech-B. Compared to the 130 mm decay results, the linear trend displayed is less adherent to the input data, particularly for the first peak and first trough. This comparative discrepancy is exacerbated in Tech-C. All accounted for, parametric transience is hypothesized.

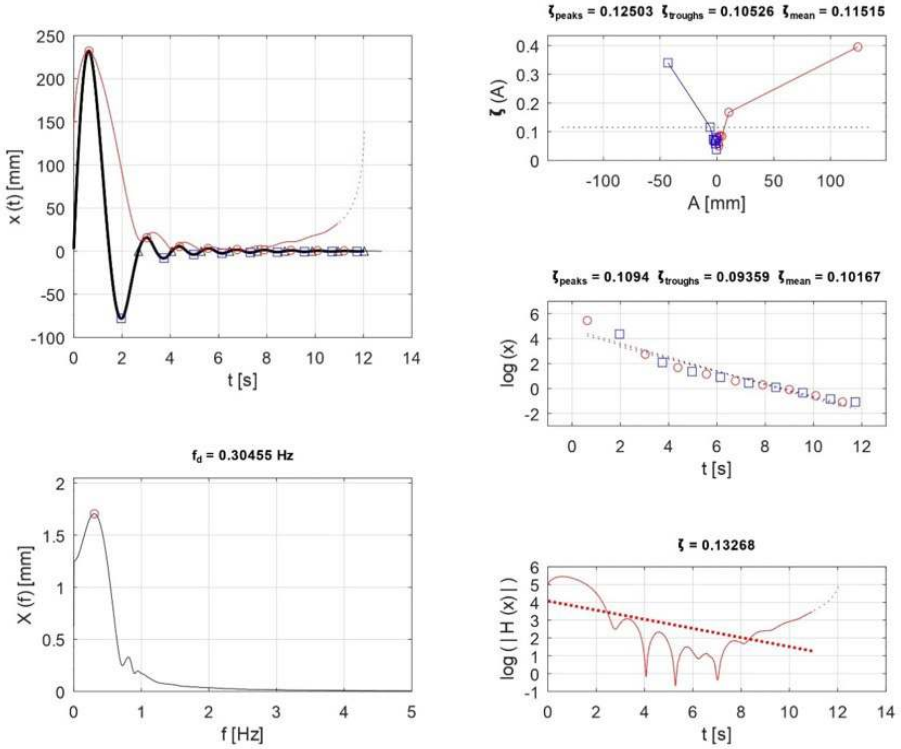


Figure 5 Umbilical cable decay test results for −450 mm initial displacement, all cycles considered.

As mentioned in this section's description paragraph, the following results are obtained from reanalysis of the last case presented. This comes as an attempt to make reason of the discrepancies that arised from the increased initial displacement imposed to the cable prior to release. As noted, the system behaved quite differently on the initial oscillation, compared to the remainder of the signal. This scenario was observed for all 450 mm decay tests. The GNU Octave routine was run again, only now beginning from the third zero crossing of the signals collected, excluding, therefore, their first oscillation's effect on the damping ratio and natural frequency estimations.

Results for the rerun 450 mm cases were by all measures similar to those obtained from the 130 mm decay tests (see Figure 6). Characteristic frequency now matched that of the smaller amplitude cases, as well as those of the second peak observed for the complete signal. Damping ratio distribution across amplitude from Tech-A now show resemblance to that in Figure 4, slightly decreasing with amplitude and condensed around a 7% overall mean. Linear regressions in Tech-B and Tech-C are again adhered to their respective input data. This "return to normality" (that reads "detection of system response analogue to that of a linear oscillator") further corroborates the hypothesis of parametric transience.

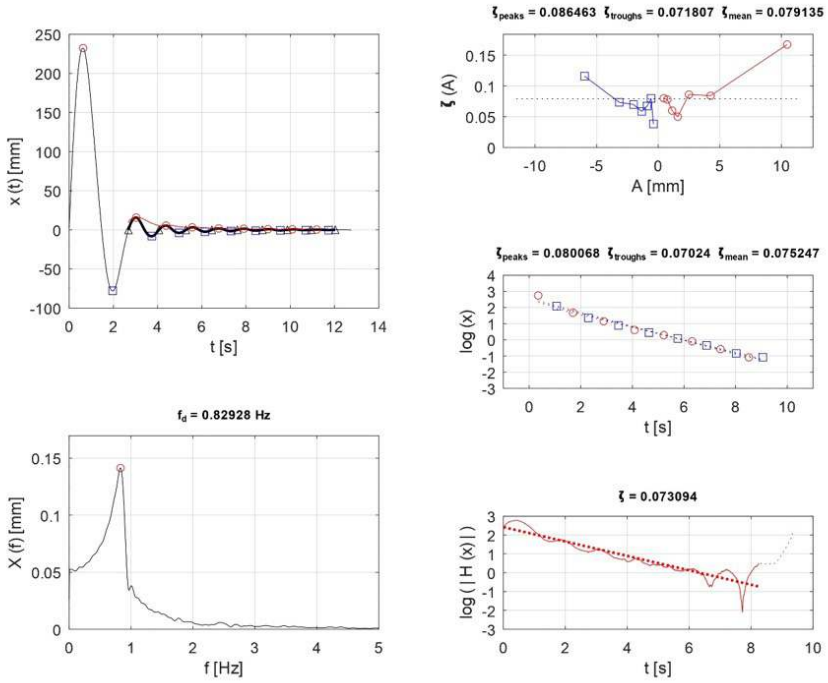


Figure 6 Umbilical cable decay test results for −450 mm initial displacement, excluding the 1st cycle.

Detailed results are presented in Table 1. It contains the data collected from all 12 decay tests. Damping ratios are shown separated by initial displacement, fraction of the signal taken into account for analysis, and technique. Results for each combination are averaged on their repetitions. Recall that the acronyms Tech A, B and C refer to the techniques applied to evaluate the damping ratio from the decay tests time-series signals: Logarithmic Decrement (Tech-A), Peak and Trough Linear Least-Square Approximation (Tech-B), and Envelope Linear Least-Square Approximation (Tech-C).

Quantitative comparison ensues. For the smaller amplitudes, mean damping ratio of 8.6% and mean frequency of 0.79 Hz were observed, along with respective bilateral asymmetries of 11.6% and 14.8% relative to their means. For the largest initial displacements, an increase in mean damping ratio to 14.5% and a drop in mean frequency to 0.31 Hz was observed. In counterpart, relative lateral asymmetries decreased to 3.3% and 7.0% respectively. This suggests that the imposition of large amplitudes of motion suppresses in some magnitude the effects of preexisting curvature.

In this context, it becomes evident that the decay tests and analysis of their respective time-series signals by standard techniques are capable of detecting changes in the systems configuration that affect damping and restoration. One limitation, however, is that this approach, as hereby conducted, cannot quantify system parameters after th**ese** transitions occur. No measurement can readily be drawn explicitly in terms of the rigidity and damping ratio evolutions during the tests. In retrospect, this means that insight into the "combination of sources" mentioned before lacks.

Table 1 Peak frequency and damping ratio for umbilical cable free decay tests.

Initial Displacement [mm]		f [Hz]	ζ [%]	
-450	Complete decay	0.3032	Tech-A	13.49
			Tech-B	12.30
			Tech-C	18.56
	Excluding 1st cycle	0.8171	Tech-A	8.97
			Tech-B	8.52
			Tech-C	8.42
-130		0.7344	Tech-A	9.41
			Tech-B	8.86
			Tech-C	8.92
+130		0.8525	Tech-A	8.42
			Tech-B	8.14
			Tech-C	7.65

Table 1 Continued…

Initial Displacement [mm]		f [Hz]	ζ [%]	
+450	Complete decay	0.3032	Tech-A	13.49
			Tech-B	12.30
			Tech-C	18.56
	Excluding 1st cycle	0.8171	Tech-A	8.97
			Tech-B	8.52
			Tech-C	8.42

To answer this demand, cyclical bending tests were conducted. These tests collect force-displacement time series, allowing the assessment of not only the per-cycle energy dissipation of the structure, but also the time- and displacement-evolution of its stiffness. These parameters are obtained by analysis of the structure's hysteretic cycle.

Figure 7 showcases results for one of such tests. As mentioned, the mean force-displacement trajectory was approximated by a bilinear cycle, then, from the geometric properties of the regressions obtained, the change in bending stiffness could be quantified. This phenomenon has been broadly documented, as presented in the cited literature. The decrease in stiffness occurs due to various types of load-induced internal accommodations of the unbonded internal components, such as inter-layer slipping, uneven straining and detachment. For the case shown (140 mm amplitude and 80 s period), a ratio of 6.4 between bending stiffnesses prior to and after accommodation was observed. Following literature nomenclature, these are referred to as "elastic" - $(EI)_e$ - and "tangential" - $(EI)_t$ - stiffnesses respectively.

Results for the cyclical bending tests are presented in Table 2.

Table 2 Damping ratio and bending stiffness ratio from umbilical cable cyclical bending tests

Amp [mm]	ζ_{eq} [%]	$(EI)_e/(EI)_t$ [-]
70	7.34	4.8
140	6.11	6.4
200	5.58	7.1

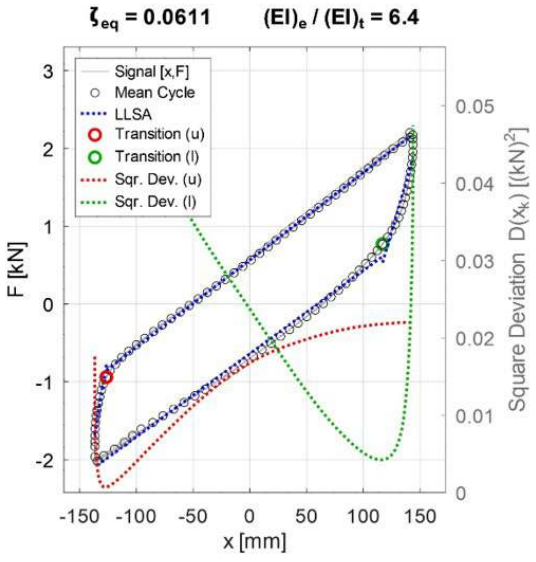


Figure 7 Umbilical cable cyclical bending test results for 140 mm amplitude, 80 s period.

Monotonic overall trends can be observed for the behaviour of the properties measured. With growing period and amplitude of imposed displacement, damping ratio decreases and bending stiffness ratio increases. The latter further corroborates the dissipation regime transition hypothesis, introduced by the observations from the free-decay tests. In this sense, the contribution of the cyclical bending tests becomes evermore evident, for it quantifies the relative change, its magnum symbol being the bending stiffness ratio $(EI)_e/(EI)_t$.

Regarding dissipation, damping ratios obtained for the cyclical bending tests differ significantly both in trend as well as in magnitude from those obtained in the decay tests. No reason for this panorama is readily apparent. Therefore, investigation followed, searching for possible sources for the discrepancy. From material origins, transience of the physical properties and internal configuration of the sample could not be evaluated, since any destructive procedures carried out on the sample prior to its testing could interfere in its behaviour. However, seen that the sample had already endured its life-span, being subjected do significantly higher demands than those imposed during testing, it was taken as very unlikely that the internal layer configuration would not have reached a so to speak structural steady-state. Furthermore, all measuring devices were calibrated prior to testing, ensuring sufficiently low measurement uncertainties.

Therefore, any possible difference should be of methodological origin. It was found that the method used for evaluating the damping ratio from the hysteretic cycle would underestimate dissipation for differing spring constants or if the fraction of the amplitude carried out in the post-slip condition is significant. This arises from a hypothesis applied in the definition of the equivalent linearly damped oscillator, for which the larger spring constant is taken as representative. What follows is the overestimation of the elastic potential energy U of the system, wich, following the energetic definition of the damping ratio, should artificially decrease its value, as seen in Equation 3, obtained from Fang and Lyons (1992).

$$\boldsymbol{\zeta = \frac{1}{4\pi}\frac{\Delta W}{U}} \tag{3}$$

A simple correction is proposed: to define the equivalent linearly damped oscillator a spring constant such that, for equal deflection amplitude, the same external work $\boldsymbol{U}$ is executed on the system. A graphical representation of this differing assumption, contrasted with its predecessor is shown in Figure 8.

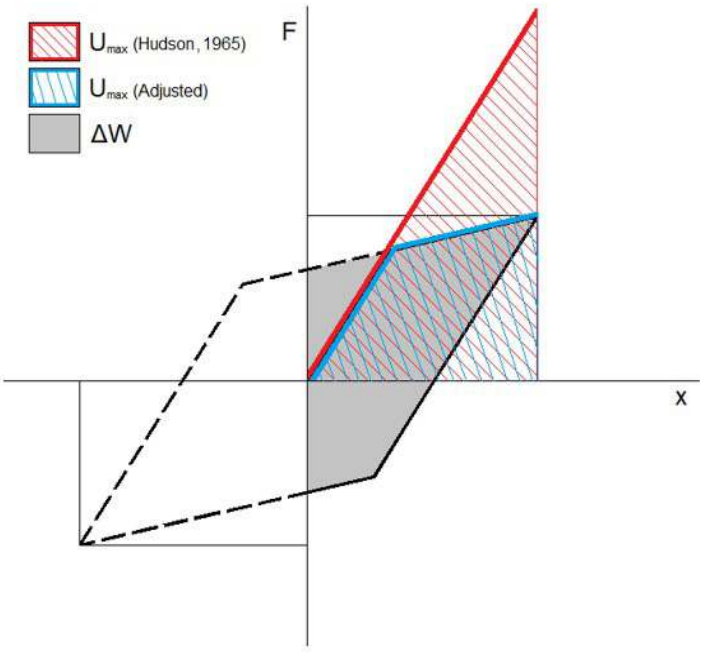


Figure 8 Adjusted maximal potential energy for the hysteretic cycle.

Since the per-cycle dissipated energy is still defined in the same way, the correction factor ψ arises from the ratio between the maximal potential energies shown, calculated from the displacements and spring constants previously obtained:

$$\boldsymbol{\psi(x', k') = \frac{1}{k'}\left(1 + \left[1 - \left(1 - \frac{1}{x'}\right)^2\right][k' - 1]\right)} \tag{4}$$

where $x' = \frac{x_m}{x_y}$, ratio between the amplitude and the characteristic yield displacement; and $k' = \frac{k_1}{k_2}$, ratio between the pre- and post-slip spring constants, respectively. The adjusted damping ratio is then given by the quotient ζ_{eq}/ψ. The correction factor ψ for each cyclical bending test is given in Figure 9.

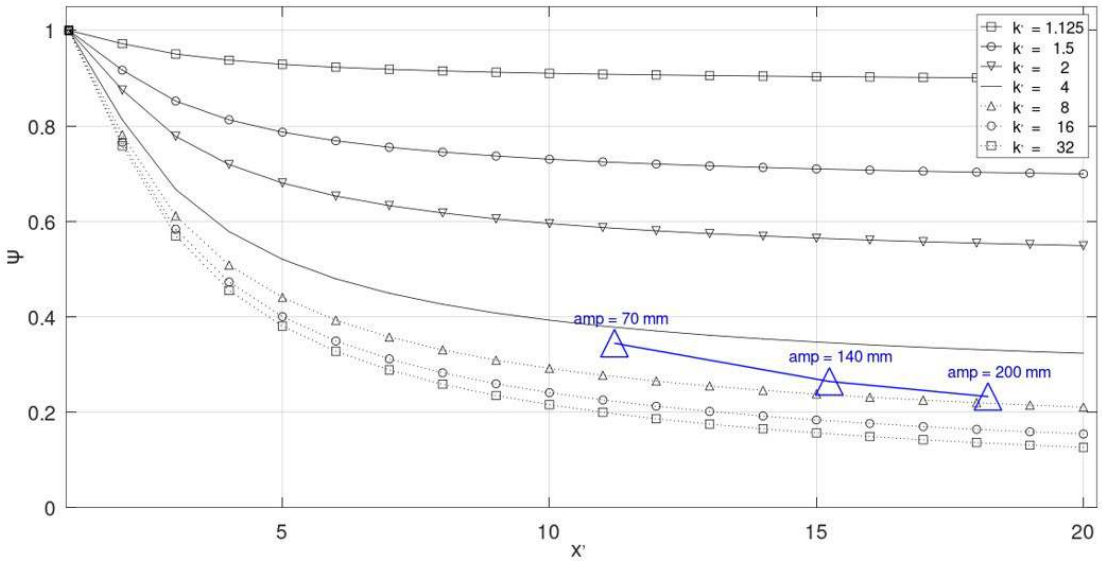


Figure 9 Mapping of the correction factor ψ for the cyclical bending tests.

The correction factors evaluate to 0.344, 0.264 and 0.232 for the 70-, 140- and 200-mm amplitude tests respectively, which gives adjusted damping ratios of 21.33%, 23.13% and 24.01%. Compared to the previous estimations, these now are significantly higher and ever so slightly increasing with amplitude. Going further back and contrasting these adjusted results to those obtained in the decay tests, values vary greatly when compared to those observed for the small amplitude free-oscillations, being now more attained to those observed during the first oscillations of the larger amplitude initial conditions.

This approximation aggregates to corroborate the high damping regime observed for larger strain conditions, where internal layer accommodation is prevalent. However, much caution must be exercised when establishing direct comparisons between the results of both tests presented. Both tests are not equivalent and the nearing of the exact values for the damping ratios should be taken as circumstantial, since test conditions are vastly different. Span, boundary conditions, characteristic periodicity, and imposed loads vary greatly. Juxtaposing results for similar amplitudes, e.g., the 130 mm decay tests and the 140 mm cyclical bending test, implies taking as true that the local strain configuration and time-dependent behaviours are equivalent for both tests, which are not.

4 CONCLUSIONS

Experimental determination of damping ratio and fundamental oscillation frequency of a real 6 m long umbilical cable sample is presented. Free-oscillation decay tests in air were conducted. Lateral displacement initial conditions of ± 130 mm and ± 450 mm were imposed. Displacement time-series were collected via a wire displacement transducer. For reliability and coherence, three techniques were applied for determination of frequencies and damping ratios. For small amplitudes, damping ratio of 8.6% and frequency of 0.79 Hz were observed. For the larger amplitudes, the damping ratio increased to 14.5% and frequencies dropped to 0.31 Hz. For these conditions, significant differences in amplitude and frequency were observed between the first oscillation and the remainder of the signal, suggesting a different damping and rigidity regime. Reanalysis followed for the larger amplitude signals, now discarding the first cycle. Damping and frequency returned to values similar to those observed for smaller initial displacement. Additionally, pre-existing curvature was observed on the umbilical, having spent its decade-long life-cycle submitted to offshore loads. This geometric lateral bias is believed to have induced slight but significant asymmetries on the measured parameters. Its effects were more pronounced in dissipation than in restoration. These lateral differences were observed to decrease for oscillations with larger initial displacements. In order to better quantify this regime transition, cyclical bending tests were conducted. Initial results for the damping ratio unexpectedly neared those observed for the smaller displacement decay tests. Investigation of the method of analysis

revealed an underestimation due to a hypothesis used in the equivalent-oscillator analysis applied. Results were adjusted and corroborating results between tests were now observed.

Acknowledgements

The authors show hereby their appreciation to the entire LIFEmu team (Laboratório de Interação Fluido Estrutura Multiusuário) at CTJ-UFSC, as well as the team at STRESSTEC, who participated in the development of this research. The fourth author, André Fujarra, also wishes to thank the Brazilian National Council for Scientific and Technological Development (CNPq) for the Research Grant 314057/2021-8.

Author's Contributions: Luiz G. de O. Appel, Lívia R. Bozzo and André L. C. Fujarra: Data analysis, result discussion, text redaction and review. Gabriel de P. Dittrich, Thiago A. Fiorentin, Andrea P. Carboni and Marcos A. Rabelo: Experiment execution. Fabio P. S. Mineiro and Carlos A. D. Lemos: Result review and discussion, text review.

Data availability statement: Research data is only available upon request.

Editor: Eduardo Alberto Fancello and Paulo de Tarso Mendonça

References

Alfano, G., Bahtui, A., Bahai, H. (2009). Numerical derivation of constitutive models for unbonded flexible risers. International Journal of Mechanical Sciences, Elsevier, v. 51, n. 4, p. 295–304.

Bech, A., Skallerud, B. (1992). Structural damping in flexible pipes: Comparisons between dynamic tests and numerical simulations. In: ISOPE International Ocean and Polar Engineering Conference. ISOPE.

Bendat, J. S., Piersol, A.G. (2010) Random Data: Analysis and Measurement Procedures, 4th edn. John Wiley & Sons, Inc., New Jersey, USA.

Clough, R. W., Penzien, J. (2003). Dynamics of Structures, 3rd edn. McGraw-Hill College, Berkeley, USA

Dong, L., Huang, Y., Zhang, Q., Liu, G. (2013). An analytical model to predict the bending behavior of unbonded flexible pipes. Journal of Ship Research, SNAME, v. 57, n. 03, p. 171–177.

Fang, J., Lyons, G. (1992). Structural damping behaviour of unbonded flexible risers. Marine Structures.

Hudson, D. E. (1965). Equivalent viscous friction for hysteretic systems with earthquake-like excitations. In: Proceedings 3rd World Conference on Earthquake Engineering, vol. 2, p. 185–202

Inman, D. J. (2014). Engineering Vibrations, 4th edn. Pearson Education, Inc., Boston, USA.

Kraincanic, I., Kebadze, E. (2001). Slip initiation and progression in helical armouring layers of unbonded flexible pipes and its effect on pipe bending behaviour. The Journal of Strain Analysis for Engineering Design, SAGE Publications Sage UK: London, England, v. 36, n. 3, p. 265–275.

Li, Z., Xu, H., Zhang, G. (2013a). Calculation methods of the local structure behavior of unbonded flexible pipes. Advanced Materials Research, Trans Tech Publ, v. 658, p. 481–486, 2013.

Li, Z., Xu, H., Zhang, G. (2013b). Analysis of structural parameters for unbonded flexible pipes. Advanced Materials Research, Trans Tech Publ, v. 652, p. 1514–1519.

Liu, J., Vaz, M. A. (2016). Viscoelastic axisymmetric structural analysis of flexible pipes in frequency domain considering temperature effect. Marine Structures 50 (2016): 111-126.

Liu, J., Vaz, M. A., Chen, R., Duan, M., Hernandez, I. (2020) Axial mechanical experiments of unbonded flexible pipes. Petroleum Science, Springer, v. 17, p. 1400–1410.

Ma, W., Su, L.; Wang, S.; Yang, Y., Huang, W. (2022) Influence of structural parameters of unbonded flexible pipes on bending performance. Ocean Engineering, Elsevier, v. 266, p. 113109.

Pesce, C. P. (1997). Mecânica de cabos e tubos submersos lançados em catenária: uma abordagem analítica e experimental. Tese (livre docente), Escola Politécnica da Universidade de São Paulo. São Paulo.

Pesce, C. P., Martins, C. A., & Chakrabarti, S. (2005). Numerical computation of riser dynamics. Numerical Models in Fluid Structure Interaction, pp. 253-309.

Santos, C. C. P., Pesce, C. P., Rabelo, M. A., Ramos Jr, R. (2015) An Assessment of HDPE Viscoelastic Behavior Effects on the Bending of Offshore Flexible Pipes. In: 23RD ABCM International Congress of Mechanical Engineering.

Witz, J. A., Tan, Z. (1992). On the flexural structural behaviour of flexible pipes, umbilicals and marine cables. Marine structures, v. 5, n. 2-3, p. 229–249.